arXiv:1512.07070v1 [nucl-ex] 22 Dec 2015

Statistical model analysis of hadron yields in proton-nucleus and heavy-ion collisions at SIS 18 energies

G. Agakishiev[7],O. Arnold[10,9], A. Balanda[3], D. Belver[18], A. Belyaev[7], J.C. Berger-Chen[10,9], A. Blanco[2], M. Böhmer[10], J. L. Boyard[16], P. Cabanelas[18],E. Castro[18], S. Chernenko[7], M. Destefanis[11],F. Dohrmann[6], A. Dybczak[3], E. Epple[10,9], L. Fabbietti[10,9], O. Fateev[7], P. Finocchiaro[1], P. Fonte[2,b], J. Friese[10], I. Fröhlich[8], T. Galatyuk[5,c], J. A. Garzón[18], R. Gernhäuser[10],C. Gilardi[11], K. Göbel[8], M. Golubeva[13], D. González-Díaz[5], F. Guber[13], M. Gumberidze[5,c], T. Heinz[4], T. Hennino[16], R. Holzmann[4], A. Ierusalimov[7], I. Iori[12,e], A. Ivashkin[13], M. Jurkovic[10], B. Kämpfer[6,d], T. Karavicheva[13], I. Koenig[4], W. Koenig[4], B. W. Kolb[4], G. Kornakov[5], R. Kotte[6], A. Krása[17], F. Krizek[17], R. Krücken[10], H. Kuc[3,16], W. Kühn[11], A. Kugler[17], A. Kurepin[13], V. Ladygin[7], R. Lalik[10,9], J. S. Lange[11], S. Lang[4], K. Lapidus[10,9], A. Lebedev[14], T. Liu[16], L. Lopes[2], M. Lorenz[8,h], L. Maier[10], A. Mangiarotti[2], J. Markert[8], V. Metag[11], B. Michalska[3], J. Michel[8], E. Morinière[16], J. Mousa[15], C. Müntz[8], R. Münzer[10,9], L. Naumann[6], Y. C. Pachmayer[8], M. Palka[3], Y. Parpottas[15,f], V. Pechenov[4], O. Pechenova[8], J. Pietraszko[4], W. Przygoda[3], B. Ramstein[16], L. Rehnisch[8], A. Reshetin[13], A. Rustamov[8], A. Sadovsky[13], P. Salabura[3], T. Scheib[8], A. Schmah[a],H. Schuldes[8], E. Schwab[4], J. Siebenson[10], Yu.G. Sobolev[17], S. Spataro[g], B. Spruck[11], H. Ströbele[8], J. Stroth[8,4], C. Sturm[4], A. Tarantola[8], K. Teilab[8], P. Tlusty[17], M. Traxler[4], R. Trebacz[3], H. Tsertos[15], T. Vasiliev[7], V. Wagner[17], M. Weber[10], C. Wendisch[4], M. Wisniowski[3], J. Wüstenfeld[6], S. Yurevich[4], Y. Zanevsky[7]

(HADES collaboration)

[1] Istituto Nazionale di Fisica Nucleare - Laboratori Nazionali del Sud, 95125 Catania, Italy
[2] LIP-Laboratório de Instrumentação e Física Experimental de Partículas , 3004-516 Coimbra, Portugal
[3] Smoluchowski Institute of Physics, Jagiellonian University of Cracow, 30-059 Kraków, Poland
[4] GSI Helmholtzzentrum für Schwerionenforschung GmbH, 64291 Darmstadt, Germany
[5] Technische Universität Darmstadt, 64289 Darmstadt, Germany
[6] Institut für Strahlenphysik, Helmholtz-Zentrum Dresden-Rossendorf, 01314 Dresden, Germany
[7] Joint Institute of Nuclear Research, 141980 Dubna, Russia
[8] Institut für Kernphysik, Goethe-Universität, 60438 Frankfurt, Germany
[9] Excellence Cluster 'Origin and Structure of the Universe' , 85748 Garching, Germany
[10] Physik Department E12, Technische Universität München, 85748 Garching, Germany
[11] II.Physikalisches Institut, Justus Liebig Universität Giessen, 35392 Giessen, Germany
[12] Istituto Nazionale di Fisica Nucleare, Sezione di Milano, 20133 Milano, Italy
[13] Institute for Nuclear Research, Russian Academy of Science, 117312 Moscow, Russia
[14] Institute of Theoretical and Experimental Physics, 117218 Moscow, Russia
[15] Department of Physics, University of Cyprus, 1678 Nicosia, Cyprus
[16] Institut de Physique Nucléaire (UMR 8608), CNRS/IN2P3 - Université Paris Sud, F-91406 Orsay Cedex, France
[17] Nuclear Physics Institute, Academy of Sciences of Czech Republic, 25068 Rez, Czech Republic
[18] LabCAF. F. Física, Univ. de Santiago de Compostela, 15706 Santiago de Compostela, Spain

[a] also at Lawrence Berkeley National Laboratory, Berkeley, USA
[b] also at ISEC Coimbra, Coimbra, Portugal
[c] also at ExtreMe Matter Institute EMMI, 64291 Darmstadt, Germany
[d] also at Technische Universität Dresden, 01062 Dresden, Germany
[e] also at Dipartimento di Fisica, Università di Milano, 20133 Milano, Italy
[f] also at Frederick University, 1036 Nicosia, Cyprus
[g] also at Dipartimento di Fisica and INFN, Università di Torino, 10125 Torino, Italy
[h] also at Utrecht University, 3584 CC Utrecht, The Netherlands

* corresponding author: m.lorenz@gsi.de

Abstract. The HADES data from p+Nb collisions at center of mass energy of $\sqrt{s_{NN}} = 3.2$ GeV are analyzed by employing a statistical model. Accounting for the identified hadrons π^0, η, Λ, K_s^0, ω allows a surprisingly good description of their abundances with parameters $T_{chem} = (99 \pm 11)$ MeV and $\mu_b = (619 \pm 34)$ MeV, which fits well in the chemical freeze-out systematics found in heavy-ion collisions. In supplement we reanalyze our previous HADES data from Ar+KCl collisions at $\sqrt{s_{NN}} = 2.6$ GeV with an updated version of the statistical model. We address equilibration in heavy-ion collisions by testing two aspects: the description of yields and the regularity of freeze-out parameters from a statistical model fit. Special emphasis is put on feed-down contributions from higher-lying resonance states which have been proposed to explain the experimentally observed Ξ^- excess present in both data samples.

1 Introduction

The idea of applying statistical methods to predict hadron yields in collisions of ions goes back to Heinz Koppe in 1948 [1] as recently pointed out in [2]. Half a century later statistical hadronization models have been established as a successful tool to describe particle yields or yield ratios from relativistic and ultrarelativistic heavy-ion collisions (HICs) [3,4,5] with only a few parameters. Moreover, the extracted freeze-out parameters show a striking regularity, lining up on a curve in the temperature - baryochemical potential plane, connecting smoothly data from the lowest energies at SIS18 up to the highest available energy at LHC [6].

These findings give a strong hint that the observed inclusive, ensemble-averaged hadron abundances correspond to (but need not to be identical with) a state described by thermal and chemical equilibrium.

Since the days of Hagedorn [7], statistical methods have also been used to predict particle production in elementary reactions, see e.g. [8]. More recently a detailed analysis applying exactly the same model [9], which successfully describes hadron yields in HICs, shows also a good agreement for yields and even transverse momentum spectra obtained in elementary $e^+ + e^-$ and $p + p$ collisions [10, 11]. [1] These findings question conclusions drawn about chemical equilibrium (either instantaneously or as time projection) in heavy-ion collisions based on the comparison of data to hadron yields obtained via statistical model calculations and ask for a more fundamental reason for the good agreement.

In this context it is important to discuss the distinctions between the different realizations of statistical models, especially their treatment of non-equilibrium parameters. While in [13,14] a grand canonical ensemble with only the parameters T (temperature) and μ_B (baryo-chemical potential) is used for central heavy-ion collisions, the authors of [9] are using a mixed canonical ensemble, conserving strangeness exactly plus an additional multiplicative factor γ_s in order to additionally suppress particles containing strangeness. In [15,16] the authors use also a mixed canonical ensemble but introduce a strangeness correlation volume parameter V_c (or correlation radius parameter R_c) instead of γ_s. In [17], on the other hand, γ_s plus an additional parameter, suppressing the light quarks u,d, called γ_q is used.

The system size and centrality dependence of those non-equilibrium parameters have been investigated in [18,19, 20]. The authors find a significant increase of the strangeness suppression factor γ_s with increasing system size.

We state that in our previous paper [21], applying a thermal fit to hadron yields obtained from Ar+KCl reactions at 1.76A GeV, we find the necessity for an additional volume parameter V_c (R_c) to further suppress strangeness and to reproduce the single-strange particles. However, the double strange Ξ^- hyperon yield overshoots the thermal fit by more than an order of magnitude. Recently, feed

down from higher-lying resonances has been proposed as a possible explanation for the observed Ξ^- excess [22]. In addition, the hadron spectrum included in the statistical model THERMUS (v2.3) [23], which we used in [21] for our Ar+KCl data, has been updated according to the report of the particle data group (PDG) 2014 [24] recently in THERMUS (v3.0).

In order to address the aspect of equilibration, we test here two aspects: the description of yields and regularity of freeze-out parameters by confronting data sets from p+Nb and Ar+KCl using the same statistical model and the same parameters. The statistical analysis of p+A represents the first of its kind in this energy regime, where usually the available yields of different particle species are limited. The HADES data allow for the first time a simultaneous fit to eight different measured yields in one experimental run. Special emphasis is put on the effect of the new states in the hadron spectrum, e.g. feed down, included in the PDG report in the last decade.

This paper is organized as follows:
We start with an overview of the two data samples in section 2, before we present and discuss the results of the statistical model fits in 3.1 and 3.2. Section 3.3 is devoted to the Ξ^- excess. Our summary is given in section 4. Finally, in the appendix we include a discussion of statistical strangeness production at high baryochemical potential using exact strangeness conservation.

2 Data sample

HADES is a charged-particle detector consisting of a 6-coil toroidal magnet centered around the beam axis and six identical detection sections located between the coils and covering polar angles between $18°$ and $85°$. Each sector is equipped with a Ring-Imaging Cherenkov (RICH) detector followed by Multi-wire Drift Chambers (MDCs), two in front of and two behind the magnetic field, as well as a scintillator hodoscope (TOF/TOFino). Hadron identification is based on the time-of-flight and on the energy-loss information from TOF/TOFino, as well as from the MDC tracking chambers. A detailed description of HADES is given in [25].

2.1 Ar+KCl at $\sqrt{s_{NN}}$= 2.6 GeV

An argon beam of $\sim 10^6$ particles/s was incident with a beam energy of 1.76A GeV on a four-fold segmented KCl target with a total thickness corresponding to 3.3 % interaction probability. A fast diamond start detector located upstream of the target was intercepting the beam and was used to determine the time-zero information. The data readout was started by a first-level trigger (LVL1) requiring a charged-particle multiplicity, $MUL \geq 16$, in the scintillator hodoscope. About 7.4×10^8 LVL1 events have been collected. The yields of the various identified particles obtained in [21,26,27,28,29,30,31,32] and their

---

[1] For completeness we refer the reader to another recent statistical analysis reaching different conclusions [12].

inverse slope parameter T_{eff} obtained from fitting Boltzmann distributions to the transverse mass spectra at midrapidity are listed in Tab. 1. The value of A_{part} is obtained by comparing the charged-particle multiplicity to the UrQMD transport model [21,33], while the yield of the η meson is interpolated from TAPS measurements in Ca+Ca collisions at 1.5 and 2A GeV [34]. The bias of the LVL2 trigger used to trigger on electrons and relevant for the ω is at the order of 10% and is corrected for.

2.2 p+Nb at $\sqrt{s_{NN}}$= 3.2 GeV

A proton beam of about 2×10^6 particles/s with kinetic energy of 3.5 GeV was incident on a 12-fold segmented target of niobium (^{93}Nb). The first-level (LVL1) trigger required a charged-particle multiplicity $MUL \geq 3$ in the scintillator hodoscope. About 3.2×10^9 LVL1 events have been collected. The yields of the various identified particles obtained in [35,36,37,38] and their inverse slope parameter T_{eff} obtained from fitting Boltzmann distributions to the transverse mass spectra are listed in Tab. 2. The value for A_{part} is obtained using a geometrical overlap model [39,40], while the 4π-yield of the ω meson is based on a GiBUU transport code which describes the data satisfactorily [39,41,42].

3 Statistical model fit to hadron yields

3.1 Ar+KCl at $\sqrt{s_{NN}}$= 2.6 GeV

We apply a similar fit as in our previous work [21] but use the updated version (v3.0) of THERMUS [23]. The main difference to the previously used version (v2.3) is the included hadron spectrum which was updated from the PDG report 2002 [43] to the one from 2014 [24], including now several new strange states, e.g. K*(800), as well as states containing charm, which are not relevant here. In addition, we include now the experimental yields of the p, ω and $K^*(892)^0$ which have become available recently [26,30,31].

We use the mixed canonical ensemble where strangeness is exactly conserved while all other quantum numbers are calculated grand canonically and constrain the charge chemical potential μ_Q using the ratio of the baryon and charge numbers of the collision system.

The yield of the ϕ meson is of particular interest, because of its sensitivity to the strangeness suppression parameters γ_s and R_c. As the ϕ conserves strangeness by definition as an $s\bar{s}$ state its yield is not suppressed in the R_c formalism, while strongly suppressed when γ_s is used. We found in [21] that the yield is well described using R_c and therefore stick to this way of suppressing strange particle yields in our statistical model calculations. Note that at higher energies and small systems the description of the ϕ meson yield improves when additional suppression parameters are introduced [16].

We fit simultaneously all particle yields listed in Tab. 1, as well as the mean number of participants $\langle A_{part}\rangle$ and constrain the charge chemical potential μ_Q. We find the following values for chemical freeze-out parameters $T_{chem} = (70 \pm 3)$ MeV, $\mu_b = (748 \pm 8)$ MeV, the strangeness correlation radius results as $R_c = (2.9 \pm 0.1)$ fm and the radius of the whole fireball $R = (5.7 \pm 0.8)$ fm with a χ^2/d.o.f. of 3.6. A detailed comparison of the data with the statistical model fit is shown in the upper part of Fig. 1, while the lower part depicts the ratio of data to the THERMUS value. In case of the Ξ^-, a number is displayed instead of a data point.

The chemical composition of particles looks as it would have a single chemical freeze-out temperature T_{chem}. At collider energies this could be the hadronization temperature at the phase boundary of the quark-gluon-plasma and a hadron gas.

These values may be compared to the values of $T_{chem} = (76 \pm 2)$ MeV, $\mu_b = (799 \pm 22)$ MeV, $R_c = (2.2 \pm 0.2)$ fm, $R = (4.1 \pm 0.5)$ fm and χ^2/d.o.f. of 2.6 obtained for the same system in [21]. We observe a deviation of all parameters at the order of a few standard deviations. While the percentaged deviation is only at the order of 5% for T and μ_b it is about 25% for the radii. Due to correlations between all four parameters the minimum of the fit moves to a slightly different position in the parameter space as a result of an interplay of several effects. As more hadron states are included, the baryochemical potential is slightly lower, which is to some extent compensated by a larger volume. Due to this larger volume the temperature T is slightly lower as otherwise the pion rate would overshoot the experimental values.

We state that we take the observed deviation of the freeze-out parameters to our previous work, as the expected systematic uncertainties of such fits.

Comparing the particle yields, the strongest deviations are observed for the protons, the η and the Ξ^-. Already the results presented in [34] pointed out that the yield of the η meson seems to favor a significantly higher freeze-out temperature. However, we want to point out that about half of its yield results of decays from baryon-resonances mainly $N(1535)$ in THERMUS.

In the sector of the vector mesons both the yields of the ω and the ϕ are in favor of a slightly higher temperature, while the $K^*(892)^0$ yield is better described with a lower temperature. The latter observation is made also at higher energies and has been interpreted as a parameter for the lifetime of the hadronic phase within the chemical freeze-out at T_{chem} and the kinetic freeze-out at T_{kin}. As due to the short life time of the $K^*(892)^0$ its decay products are rescattered inside the medium [44], while for instance the decay products of the ϕ meson are not affected, as the ϕ decays mainly outside of the medium due to its longer life time.

The worse χ^2/d.o.f. compared to the previous fit [21] results mainly from the inclusion of the Ξ^-. The excess of the experimentally measured Ξ^- yield over the model decreases from a factor 24±9 to a factor 15±6 when using the actual version (v3.0) of THERMUS. We will come back to this in the discussion of the Ξ^- excess.

Table 1. Multiplicities (i.e. yield/LVL1 event) and effective temperatures T_{eff} of particles produced in Ar(1.76A GeV)+KCl reactions. If only a single error is given, the value corresponds to the total error, including systematic and statistical uncertainties. A "$-$" in the T_{eff} column means that the spectra are too scarce to extract a value.

Particle	Multiplicity	T_{eff} [MeV]	Reference
$\langle A_{part} \rangle$	38.5 ± 4	$-$	[21, 33]
p	22.11 ± 2.4	142 ± 5	[26]
π^-	$3.9 \pm 0.19 \pm 0.34(syst)$	$82.4 \pm 0.1^{+9.1}_{-4.6}$	[27]
η	0.081 ± 0.02	$-$	[34]
$\Lambda + \Sigma^0$	$(4.09 \pm 0.1 \pm 0.17(extr)^{+0.17}_{-0.37}(syst)) \times 10^{-2}$	$95.5 \pm 0.7 + 2.2$	[21]
K^+	$(2.8 \pm 0.2 \pm 0.1(syst) \pm 0.1(extr)) \times 10^{-2}$	$89 \pm 1 \pm 2$	[28]
K^0_S	$(1.15 \pm 0.05 \pm 0.09(syst)) \times 10^{-2}$	92 ± 2	[29]
K^-	$(7.1 \pm 1.5 \pm 0.3(syst) \pm 0.1(extr)) \times 10^{-4}$	$69 \pm 2 \pm 4$	[28]
$K^*(892)^0$	$(4.4 \pm 1.1 \pm 0.5(syst)) \times 10^{-4}$	$-$	[30]
ω	$(6.7 \pm 2.7) \times 10^{-3}$	131 ± 26	[31]
ϕ	$(2.6 \pm 0.7 \pm 0.1 - 0.3) \times 10^{-4}$	84 ± 8	[28]
Ξ^-	$(2.3 \pm 0.9) \times 10^{-4}$	$-$	[32]

Table 2. As in Tab. 1 but for p(3.5GeV)+Nb reactions.

Particle	Multiplicity	T_{eff} [MeV]	Reference
$\langle A_{part} \rangle$	2.8 ± 0.6	$-$	[39, 40]
π^0	$0.66 \pm 0.06 \pm 0.1(syst)$	92 ± 3 combined fit with π^-	[35]
π^-	0.6 ± 0.1	92 ± 3 combined fit with π^0	[35]
η	$0.034 \pm 0.002 \pm 0.008(syst)$	84 ± 3	[35]
$\Lambda + \Sigma^0$	0.017 ± 0.003	92 ± 5	[36]
K^0_S	0.0055 ± 0.0007	99 ± 4	[37]
ω	0.007 ± 0.004	$-$	[39, 41, 42]
Ξ^-	$(2.0 \pm 0.4 \pm 0.6(syst)) \times 10^{-4}$	$-$	[38]

The comparison of the extracted chemical freeze-out temperature T_{chem} to the ones extracted from the inverse slope T_{eff} of transverse mass spectra at mid-rapidity for various particles listed in Tab. 1 is not straightforward. In a naive picture the extracted inverse slope parameter T_{eff} include a pure kinetical component T_{kin} plus an additive term, depending on the particle mass m and the square of the radial expansion velocity β. In addition effects like resonance decays deform the spectra complicating this naive interpretation.

3.2 p+Nb at $\sqrt{s_{NN}} = 3.2$ GeV

For the fit to the yields obtained from p+Nb reactions we add the charge chemical potential μ_Q as an additional free parameter due to the strong asymmetry of the collision system. Apart from the charge chemical potential μ_Q, we use the same parameters as above. The extracted parameters are $T_{chem} = (99 \pm 11)$ MeV, $\mu_b = (619 \pm 34)$ MeV, $\mu_Q = (18 \pm 18)$ MeV, $R_c = (1.5 \pm 0.8)$ fm, $R = (2.0 \pm 0.6)$ fm and χ^2/d.o.f. of 2.9. A detailed comparison of the data with the statistical model fit is shown in the upper part of Fig. 2, while the lower part of this figure depicts the ratio of data to THERMUS values. Again, in case of the Ξ^-, a number is displayed instead of a point. Within errors, the values for R and R_c agree with each
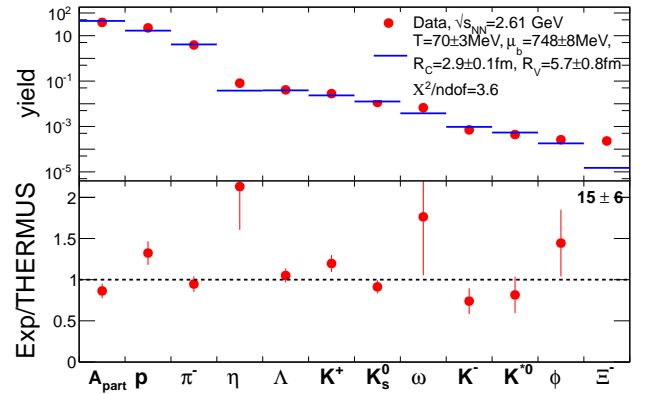

Fig. 1. Yields (filled red circles) of hadrons in Ar+KCl reactions and the corresponding THERMUS fit values (blue bars). The lower plot shows the ratio of the experimental value and the THERMUS value. For the Ξ^- the ratio number is quoted instead of a point.

other, which one expects as the suppression of strange particles compared to non strange particles depends mostly on the absolute value of R_c and only very weakly on the ratio of R_c/R.
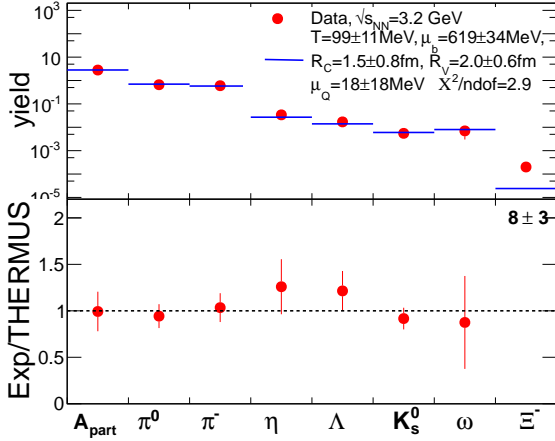
Fig. 2. Yields of hadrons in p+Nb reactions (filled red circles) and the corresponding THERMUS fit (blue bars). The lower plot shows the ratio of the experimental value and the THERMUS value. For the Ξ^- the ratio number is quoted instead of displaying a point.

Fig. 3. As in Fig. 1 but excluding the p, K^+, K^-, $K^*(892)^0$, ϕ yields, shown by open symbols, in the fit.

The ratio between data and model show striking similarities when comparing the Ar+KCl values in Fig. 1 with the ones of p+Nb in Fig. 2. In both cases the model is able to describe with fair agreement most of the yields but fails by nearly an order of magnitude in case of the Ξ^-.

Similar as for the Ar+KCl fit the excess of the experimentally measured Ξ^- yield over the model decreases from a factor 20 ± 9 as reported in [38] to a factor 8 ± 3 when using the current THERMUS version (v3.0).

The comparison of the extracted chemical freeze-out temperature T_{chem} to the ones extracted from the inverse slopes of transverse mass spectra at mid-rapidity for various particles listed in Tab. 2 is more straight forward than in case of Ar+KCl, as we expect no collective expansion of the system. Indeed the extracted slopes show no significant dependence on the particle mass with an average value of $\langle T_{kin} \rangle = (91 \pm 2)$ MeV, which is in agreement with the value for the chemical freeze-out temperature extracted from the statistical fit of $T_{chem} = (99 \pm 11)$ MeV.

In order to further discuss the similarities between the Ar+KCl and the p+Nb fit, we reduce our larger Ar+KCl data sample to the same set of identified hadron species as in the p+Nb sample, by excluding the yields of the p, K^+, K^-, $K^*(892)^0$ and the ϕ in our fit. [2] For the reduced Ar+KCl fit we find $T_{chem} = (80 \pm 14)$ MeV, $\mu_b = (749 \pm 12)$ MeV, $R_c = (1.9 \pm 0.1)$ fm, $R = (4.2 \pm 0.2)$ fm and χ^2/d.o.f. of 2.5. The comparison between data and model is shown in a similar way as above in Fig. 3.

By restricting the Ar+KCl sample to a comparable one as available for p+Nb we find a variation of the freeze-out parameters of order 5%, which we attribute to the systematic uncertainties of such an analysis.

The χ^2/d.o.f. of the Ar+KCl fits of 3.6 and 2.5 are comparable to the one obtained for the p+Nb sample of 2.9. This is rather surprising as one naively expects a larger amount of thermalization in the larger Ar+KCl system and hence less deviation from statistical equilibrium values. Note that the average number of participants is smaller than 3 in case of the p+Nb sample. Furthermore, the p+Nb freeze-out point fits at least as well as the Ar+KCl points to the previously observed regularity of freeze-out points in the $T_{chem} - \mu_b$ plane, displayed in Fig. 4, where the extracted points of this work are displayed together with similar points extracted in [6,13,14].

This brings us back to the motivation of our analysis stressed in the introduction: While the success of the statistical model in describing particle rates from heavy-ion collisions is often implicitly connected to a thermalization of the created system, the success of the model for the p+Nb data at $\sqrt{s_{NN}} = 3.2$ GeV questions this connection.

Apart from such conceptional issues we stress that T_{chem} for p+Nb at $\sqrt{s_{NN}} = 3.2$ GeV is "naturally" somewhat larger than T_{chem} for Ar+KCl at $\sqrt{s_{NN}} = 2.6$ GeV which one could attribute to the higher energies in first-chance collisions producing secondary hadrons. Analogously, μ_b in Ar+KCl is larger than for p+Nb, since some noticeable compression is expected in heavy-ion collisions. On the other hand, the authors of [45] find only a very small dependence on the system size of T_{chem} and μ_b for SPS energies and hence conclude that both parameters are mainly determined by the energy of the incoming projectile.

3.3 On the Ξ^- puzzle

The presence of the excess of the Ξ^- also in cold nuclear matter has several interesting implications for the interpretation of the heavy-ion data as its origin seems to be already in the elementary channels without the involvement of many-body effects in the medium. Therefore, the

---

[2]   As the yield of the neutral pions is not directly available, we restrict μ_Q by the initial neutron to proton ratio.

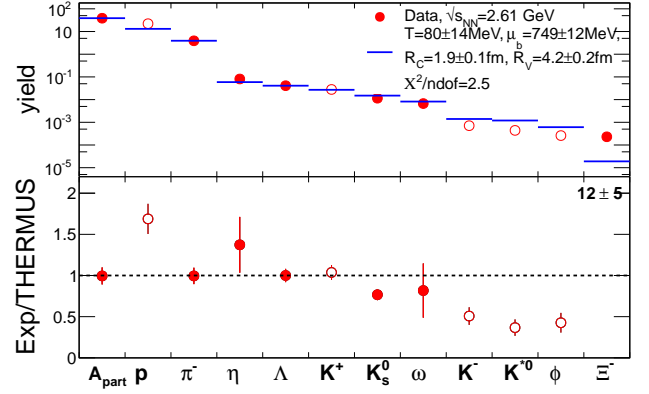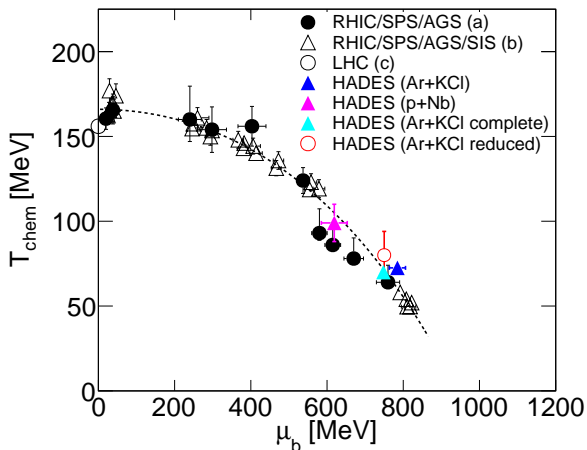**Fig. 4.** Chemical freeze-out points in the $T_chem - \mu_b$ plane. The filled black circles (a) are taken from [13], the black open triangles (b) are from [6] and the black open circle (c) from [14]. The presented fit results are defined in the legend. The dashed curve correponds to a fixed energy per nucleon of 1 GeV, calculated according to [6]. The dark blue triangle corresponds to our Ar+KCl fit presented in [21], the light blue triangle shows the result obtained for the full sample and open circle to the reduced data sample both presented in this work.

increased cross sections of strangeness exchange reactions, which were found to be sufficient to explain the high yield in [46,47], seem to be questionable as they are unlikely to play an important role in p+Nb reactions. Also the invoked [48] catalytic strangeness production by secondary processes, such as $\pi + Y \rightarrow \Xi + K$, are strongly suppressed in cold nuclear matter.

Feed down from the high-mass tails of resonances has been proposed as another possible explanation recently in [22]. The authors tuned the mass depending branching ratio of high-lying baryon resonances, namely the $N^*(1990)$, $N^*(2080)$, $N^*(2190)$, $N^*(2220)$ and $N^*(2250)$, in a transport code to match elementary data on ϕ meson production. As a result the ϕ/K^- ratio in Ar+KCl is successfully reproduced. The same mechanism is then also used for the Ξ^- hyperon but due to the lack of elementary data the model is tuned to match our p+Nb data.

The technique of mass dependent branching ratios for broad resonances has been successfully applied in order to describe the dilepton spectra at low energies as pointed out in [41,52]. Although the tuned branching ratios are still consistent with the OZI rule there is no experimental evidence for the decay of the N^* resonance to final states containing a ϕ meson or a Ξ hyperon. Therefore, there is no branching of N^* resonances to double-strange final states included in THERMUS.

In addition, the total yield of the five above discussed N^* resonances amounts to 1.47×10^{-3} and 7.1×10^{-4} in THERMUS for the Ar+KCl and the p+Nb data sample respectively. In order to explain the observed Ξ^- yields which are at the order of 10^{-4} in both systems, branching ratios of the N^* resonances to Ξ^- at the order of 10% or higher would be needed. This seems to be unreasonably high.

Instead, the feed down to Ξ hyperons is mainly originating from the decay of excited $\Xi(1530,1690,1820,1950,2030)$ and some higher-lying Λ and Σ states. Note that the widths, branching ratios etc. of these states are not well constrained and subject of current and future scientific activities [53,54]. The feed down fraction to the Ξ^- yield amounts to 10% and 27% percent of the total rate in THERMUS respectively for Ar+KCl and p+Nb. From these numbers it becomes clear that the difference in yields of the double-strange hyperons of about 50% between the two used THERMUS versions is not due to additional higher-lying states and corresponding feed-down. Instead, the difference is connected to the new states in the hadron spectrum via the mechanism for exact strangeness conservation using the strangeness correlation volume V_c. As there are more hadronic (mesonic) states included in the current version, the probability for counterbalancing the strange quarks of the hyperons is higher for a given volume. Especially the rather low-lying scalar meson $K^*(800)^{0+}$ (also known as κ) is important in this context as its abundance is still not too rare. However, one should note that, with a widths of $\Gamma \approx 500$ MeV evidences for this state are hard to establish. The effect on the yield is much more prominently seen in the double-strange baryon sector because their yield scales with the volume proportional to the power of three, see Eq. (6) compared to the one of single-strange particles whose yield scales only quadratically with the volume, see Eq. (5).

From this consideration it becomes clear that a precise knowledge of the hadron spectrum is an important issue for the interpretation of HIC data.

4 Summary and Outlook

By comparing the obtained freeze-out parameters from a statistical model fit to HADES data obtained from p+Nb and Ar+KCl collisions at center of mass energies of $\sqrt{s_{NN}}$ = 3.2 GeV and $\sqrt{s_{NN}}$ = 2.6 GeV respectively, we tried to address the aspect of equilibration in HIC by testing two manifestations, the description of yields and regularity of freeze-out parameters. We make the rather surprising finding that the statistical model is able to describe the p+Nb data as well as the larger system the Ar+KCl data, which questions the often drawn connection between the agreement of statistical models with particle yields in heavy-ion collisions and thermalization.

Furthermore, we emphasize that the excess of the Ξ^- is already present in cold nuclear matter. Given the rates of higher-lying N^* resonances predicted by our statistical model fit, we find feed down of these states a rather implausible explanation for the excess of the Ξ^- yield over the model value. In addition, we state the importance of a precise knowledge of the hadron spectrum for interpretation of HIC data.

We want to point out that HADES data of central Au+Au collisions will be available soon and might allow to gather further insights into the subject.

References

1. H. Koppe, Z. Naturforschg. 3 a, 251 (1948).
2. A. N. Tawfik, Z. Naturforschg. 69a, 106 (2014).
3. P. Braun-Munzinger, K. Redlich and J. Stachel, arXiv:nucl-th/0304013 (2003).
4. A. N. Tawfik, Int. J. Mod. Phys. A **29**, 1430021 (2014).
5. M. Floris, Nucl. Phys. A **931**, 103 (2014).
6. J. Cleymans, H. Oeschler, K. Redlich and S. Wheaton, Phys. Rev. C **73**, 034905 (2006).
7. R. Hagedorn, Nuovo Cim. Suppl. **3**, 147 (1965).
8. E. V. Shuryak, Yad. Fiz. **16**, 395 (1972).
9. F. Becattini, M. Gazdzicki, A. Keranen, J. Manninen and R. Stock, Phys. Rev. C **69**, 024905 (2004).
10. F. Becattini and G. Passaleva, Eur. Phys. J. C **23**, 551 (2002).
11. F. Becattini, P. Castorina, J. Manninen and H. Satz, Eur. Phys. J. C **56**, 493 (2008).
12. A. Andronic, F. Beutler, P. Braun-Munzinger, K. Redlich and J. Stachel, Phys. Lett. B **675**, 312 (2009).
13. A. Andronic, P. Braun-Munzinger and J. Stachel, Nucl. Phys. A **772**, 167 (2006).
14. J. Stachel, A. Andronic, P. Braun-Munzinger and K. Redlich, J. Phys. Conf. Ser. **509**, 012019 (2014).
15. J. Cleymans *et al.*, Phys. Rev. C **59**, 1663 (1999).
16. I. Kraus, J. Cleymans, H. Oeschler, K. Redlich and S. Wheaton, Phys. Rev. C **76**, 064903 (2007).
17. M. Petran, J. Letessier, V. Petracek and J. Rafelski, Phys. Rev. C **88**, 034907 (2013).
18. J. Cleymans, B. Kämpfer, P. Steinberg and S. Wheaton, J. Phys. G **30**, S595 (2004).
19. B. Kämpfer, J. Cleymans, P. Steinberg and S. Wheaton, Heavy Ion Phys. **21**, 207 (2004).
20. J. Cleymans, B. Kampfer, M. Kaneta, S. Wheaton and N. Xu, Phys. Rev. C **71**, 054901 (2005).
21. G. Agakishiev *et al.* [HADES Collaboration], Eur. Phys. J. A **47**, 21 (2011).
22. J. Steinheimer and M. Bleicher, arXiv:1503.07305 [nucl-th].
23. S. Wheaton and J. Cleymans, Comput. Phys. Commun. **180**, 84 (2009).
24. K. A. Olive *et al.* [Particle Data Group Collaboration], Chin. Phys. C **38**, 090001 (2014).
25. G. Agakishiev *et al.* [HADES Collaboration], Eur. Phys. J. A **41**, 243 (2009).
26. H. Schuldes *et al.* [HADES Collaboration], J. Phys. Conf. Ser. **599**, 012028 (2015).
27. P. Tlusty *et al.* [HADES Collaboration], arXiv:0906.2309 (2009).
28. G. Agakishiev *et al.* [HADES Collaboration], Phys. Rev. C **80**, 025209 (2009).
29. G. Agakishiev *et al.* [HADES Collaboration], Phys. Rev. C **82**, 044907 (2010).
30. G. Agakishiev *et al.* [HADES Collaboration], Eur. Phys. J. A **49**, 34 (2013).
31. G. Agakishiev *et al.* [HADES Collaboration], Phys. Rev. C **84**, 014902 (2011).
32. G. Agakishiev *et al.* [HADES Collaboration], Phys. Rev. Lett. **103**, 132301 (2009).
33. S. A. Bass *et al.*, Prog. Part. Nucl. Phys. **41**, 225 (1998).
34. R. Averbeck, R. Holzmann, V. Metag and R. S. Simon, Phys. Rev. C **67**, 024903 (2003).
35. G. Agakishiev *et al.* [HADES Collaboration], Phys. Rev. C **88**, 024904 (2013).
36. G. Agakishiev *et al.* [HADES Collaboration], Eur. Phys. J. A **50**, 81 (2014).
37. G. Agakishiev *et al.* [HADES Collaboration], Phys. Rev. C **90**, 054906 (2014).
38. G. Agakishiev *et al.* [HADES Collaboration]. Phys. Rev. Lett. **114**, 212301 (2015).
39. G. Agakishiev *et al.* [HADES Collaboration], Phys. Lett. B **715**, 304 (2012).
40. R. J. Glauber and G. Matthiae, Nucl. Phys. **B 21**, 135 (1970).
41. J. Weil, H. van Hees and U. Mosel, Eur. Phys. J. A **48**, 111 (2012).
42. J. Weil, private communication.
43. K. Hagiwara et al. (Particle Data Group), Phys. Rev. D **66**, 010001 (2002).
44. C. Markert, G. Torrieri and J. Rafelski, AIP Conf. Proc. **631**, 533 (2002).
45. F. Becattini, J. Manninen and M. Gazdzicki, Phys. Rev. C **73**, 044905 (2006).
46. F. Li, L. W. Chen, C. M. Ko and S. H. Lee, Phys. Rev. C **85**, 064902 (2012).
47. G. Graef, J. Steinheimer, F. Li and M. Bleicher, Phys. Rev. C **90**, 064909 (2014).
48. E. E. Kolomeitsev, B. Tomasik and D. N. Voskresensky, Phys. Rev. C **86**, 054909 (2012) .
49. M. Lorenz *et al.* (HADES Collaboration), PoS (BORMIO2010) 038 (2010).
50. K. Piasecki *et al.* [FOPI Collaboration], Phys. Rev. C **91**, 054904 (2015).
51. Y. Cheng, F. Liu, Z. Liu, K. Schweda and N. Xu, Phys. Rev. C **68**, 034910 (2003).
52. E. L. Bratkovskaya, J. Aichelin, M. Thomere, S. Vogel and M. Bleicher, Phys. Rev. C **87**, 064907 (2013).
53. M. Ronniger and B. Ch. Metsch, Eur. Phys. J. A **47**, 162 (2011).
54. M.F.M. Lutz *et al.* [PANDA Collaboration], arXiv:0903.3905 (2009).

A Statistical strangeness production at high baryo-chemical potential using exact strangeness conservation

In a pure statistical ansatz based on the common temperature T of all species and the baryo-chemical potential μ_B, the multiplicities of mesons and baryons produced in a heavy-ion collision, neglecting feed-down and isospin asymmetry are given by

$$\sum_i M_{m_i} = \sum_i g_i V \int \frac{d^3 p}{(2\pi)^3} \exp\left(-\frac{E_i}{T}\right) \times F_{Si}, \quad (1)$$

$$\sum_j M_{b_j} = \sum_j g_j V \int \frac{d^3 p}{(2\pi)^3} \exp\left(-\frac{E_j - \mu_B}{T}\right) \times F_{Sj}, \quad (2)$$

with M_{m_i} and M_{b_j} being the multiplicities of a given meson (m) or baryon (b), the degeneracy factors $g_{i,j}$, the volume of the fireball V and the energies of the corresponding meson and baryon $E_{i,j} = \sqrt{m_{i,j}^2 + p_{i,j}^2}$.

Particles containing strangeness are rare, especially at SIS energies, and therefore the strange quantum number must be exactly conserved in each event in the ensemble; each particle carrying a strange quark must be counterbalanced by one carrying an antistrange quark due to associated strangeness production in strong-interaction processes. This results in a multiplicative canonical suppression factor $F_S(T, \mu_B, V, S, N_S)$, which is equal to one for non-strange particles and approaches, in the limit of large volumes and temperatures, the grand canonical fugacities $\lim_{V,T\to\infty} F_{Si,j} = exp\left(-S_{i,j}\mu_S/T\right)$. The factor $F_{Si,j}$ for each particle species i, j depends in general on the thermodynamical properties of the system, the strangeness content $S_{i,j}$ of the respective particle and the number of meson and baryon states containing strangeness N_S.

We illustrate the effect of F_S by making use of the opposite limit of small volume and temperature, where particle numbers are small and the canonical strangeness suppression is most relevant. For $M < 1$ and neglecting higher order effects, the multiplicity of kaons M_{m_K} can be approximated as

$$M_{m_K} \approx g_K V \int \frac{d^3 p}{(2\pi)^3} \exp\left(-\frac{E_K}{T}\right) \times \left[g_Y V \int \frac{d^3 p}{(2\pi)^3}\right.$$
$$\left. \exp\left(-\frac{E_Y - \mu_B}{T}\right) + g_{\overline{K}} V \int \frac{d^3 p}{(2\pi)^3} \exp\left(-\frac{E_{\overline{K}}}{T}\right)\right]. \quad (3)$$

The two terms inside the square brackets correspond to the counterbalance terms for the antistrange quark inside the kaons from the hyperons and from the antikaons. Hence Eq. (3) can be rewritten as

$$M_{m_K} \approx M_{m_K}^{GC} \times \left[M_{m_Y}^{GC} + M_{m_{\overline{K}}}^{GC}\right] \quad (4)$$

with $M_{b_Y}^{GC}$, $M_{m_K}^{GC}$ and $M_{m_{\overline{K}}}^{GC}$ corresponding to the grand-canonical multiplicities of kaons, hyperons and antikaons, respectively. As we assume T and V to be sufficiently small, so that $M < 1$, one can clearly see the resulting suppression due to exact strangeness conservation. Due to the absence of antimatter at high μ_B the counterbalance term for the antikaons by the antihyperons is missing, resulting in a stronger suppression compared to kaons. Hence for $(E_Y - \mu_B) \ll E_K$ we can neglect the antikaon term and approximate the multiplicity of single-strange hyperons as

$$M_{b_Y} \approx M_{b_Y}^{GC} \times \left[M_{m_K}^{GC}\right] \propto V^2. \quad (5)$$

Compared to non-strange particle multiplicities, which are proportional to V the multiplicity of single-strange particles is proportional to V^2 for small systems. Rewriting Eq. (5) for double-strange hyperons, like the Ξ, one finds their yield scaling with V^3:

$$M_{b_\Xi} \approx M_{b_\Xi}^{GC} \times \left[M_{m_K}^{GC}\right]^2 \propto V^3. \quad (6)$$

The above mentioned strangeness correlation volume V_c, in which strangeness has to be exactly conserved, is realized by setting the volume terms in the brackets in Eq. (3) to V_c. For $V_c < V$, strange particles are suppressed additionally on top of the pure canonical suppression.

From these considerations it becomes clear that the size of F_S for a given volume V_c and hence the strength of the suppression depends also on the number of known strange particle states. The more states exist the more possibilities are available for counterbalancing the strange (antistrange) quarks. This is of relevance for the comparison of the different THERMUS versions 2.3 and 3.0. The latter one has more states included, especially the rather low lying K*(800) states are important in this context.